

RESEARCH ARTICLE | MARCH 01 2024

A molecular dynamics study on the boundary between homogeneous and heterogeneous nucleation

Hua Men  



J. Chem. Phys. 160, 094702 (2024)

<https://doi.org/10.1063/5.0192069>

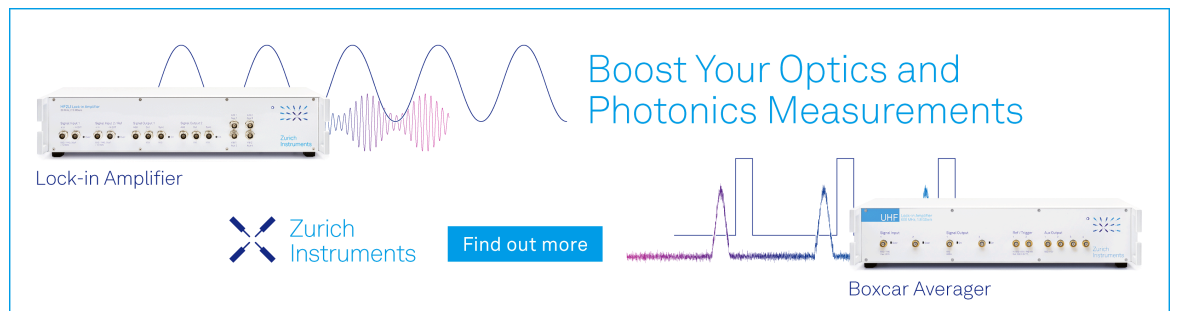


View
Online




Export
Citation

CrossMark



Boost Your Optics and Photonics Measurements

Lock-in Amplifier

 Zurich Instruments

[Find out more](#)

Boxcar Averager

A molecular dynamics study on the boundary between homogeneous and heterogeneous nucleation

Cite as: *J. Chem. Phys.* **160**, 094702 (2024); doi: [10.1063/5.0192069](https://doi.org/10.1063/5.0192069)

Submitted: 18 December 2023 • Accepted: 17 February 2024 •

Published Online: 1 March 2024



View Online



Export Citation



CrossMark

Hua Men^{a)} 

AFFILIATIONS

BCAST, Brunel University London, Uxbridge, Middlesex UB8 3PH, United Kingdom

^{a)} Author to whom correspondence should be addressed: hua.men@brunel.ac.uk

ABSTRACT

The large discrepancy among the nucleation kinetics extracted from experimental measurements and computer simulations and the prediction of the classical nucleation theory (CNT) has stimulated intense arguments about its origin in the past decades, which is crucially relevant to the validity of the CNT. In this paper, we investigate the atomistic mechanism of the nucleation in liquid Al in contact with amorphous substrates with atomic-level smooth/rough surfaces, using molecular dynamics (MD) simulations. This study reveals that the slightly distorted local fcc/hcp structures in amorphous substrates with smooth surfaces can promote heterogeneous nucleation through a structural templating mechanism, and on the other hand, homogeneous nucleation will occur at a larger undercooling through a fluctuation mechanism if the surface is rough. Thus, some impurities, previously thought to be impotent, could be activated in the homogeneous nucleation experiments. We further find that the initial growth of the nucleus on smooth surfaces of amorphous substrates is one order of magnitude faster than that in homogeneous nucleation. Both these factors could significantly contribute to the discrepancy in the nucleation kinetics. This study is also supported by a recent study of the synthesis of high-entropy alloy nanoparticles assisted with the liquid metal Ga [Cao *et al.*, *Nature* **619**, 73 (2023)]. In this study, we established that the boundary existed between homogeneous and heterogeneous nucleation, i.e., the structural templating is a general mechanism for heterogeneous nucleation, and in its absence, homogeneous nucleation will occur through the fluctuation mechanism. This study provides an in-depth understanding of the nucleation theory and experiments.

© 2024 Author(s). All article content, except where otherwise noted, is licensed under a Creative Commons Attribution (CC BY) license (<http://creativecommons.org/licenses/by/4.0/>). <https://doi.org/10.1063/5.0192069>

I. INTRODUCTION

Nucleation as the first step of solidification in liquid is often poorly understood, compared to growth, although it is fundamentally important in controlling the quality of the castings to achieve a fine and uniform microstructure.¹ Homogeneous nucleation is rarely observed in nature due to the inevitable presence of some nucleants (impurities) in the liquid. Instead, heterogeneous nucleation will occur in these nucleants.^{1,2} The potency of a nucleant depends on the matching between the surface of the nucleant and the new phase, and in general, it degrades by increasing the lattice misfit.³ One wonders whether or not the nucleant can become impotent, while the mismatching continues to grow and then homogeneous nucleation will start.² To put it another way, how can a real liquid be

recognized as free of the nucleant, and so, homogeneous nucleation is solely responsible for the solidification?

This question is fundamentally important in the research field of nucleation theory since the nucleation rate obtained from the experiments or computer simulations on homogeneous nucleation is the most important factor to test the validity of the classical nucleation theory (CNT).^{4,5} Substantial disagreements exist among the data extracted from the experimental measurements and computer simulations and the prediction of the CNT.^{6,7} One of the important uncertainties in the experiments is whether the nucleation is really homogeneous. It often claims that the nucleation in the experimental measurements is homogeneous as the impurities in the liquids have been reduced as much as possible with advanced techniques, such as fluxing or droplet levitation.^{8–11} However, with advance-

ment in the techniques, larger and larger undercooling has been achieved for pure liquid metals,^{11,12} indicating that many so-called homogeneous nucleations in early experiments are actually heterogeneous. On the other hand, homogeneous nucleation is definitely achievable in the computer simulations although the simulation has its own problem; for instance, the nucleation is a rare event and the nucleation rate is highly related to the system size used in the simulations.⁶ Therefore, it is desirable to establish the boundary between homogeneous and heterogeneous nucleation with the computer simulations, in terms of the role of the nucleant (substrates) in solidification.

The substrates can induce prenucleation in the liquid at the interface, i.e., the profound atomic ordering, including the layering, in-plane atomic ordering,^{13–23} and the two-dimensional (2D) ordered structure,^{21,23} even above the melting point (T_m). The atomic layering is attributed to the “hard wall” effect,^{24,25} and its significance depends on the atomic-level roughness of the substrate.^{26,27} The in-plane atomic ordering results from a structural templating mechanism and is largely related to the matching with the substrate lattice.^{21,28} Atomistic simulations can provide microscopic details of the liquid/solid (substrate) interfaces. In the molecular dynamics (MD) simulation with adapted n -body potentials, Geyermans *et al.*²⁶ reported the significant layering in liquid Al adjacent to a solid Cu wall, which was largely independent of surface orientation of the Cu substrates. Using the embedded atom method (EAM) potential, Hashibon *et al.*^{17,18} revealed that the in-plane atomic ordering in liquid Al in contact with a bcc (100) substrate was far greater than that with a bcc (110) substrate. Palafox–Hernandez *et al.*^{19,29} observed that 2–3 “prefreezing” layers existed in liquid Pb at the interface with a solid Cu (111) plane, where the lattice spacing of the “prefreezing” Pb layers was 33% larger than the Cu substrate. Nevertheless, Yang *et al.*³⁰ reported that there was no prefreezing layer in the liquid Pb at the interface with an Al substrate, in which the lattice misfit (f) between the solid Pb and Al was 18.2%. Here, the lattice misfit is defined as $f = (d_{\text{solid}} - d_{\text{substrate}})/d_{\text{solid}}$, where d_{solid} and $d_{\text{substrate}}$ are the atomic spacings along the close-packed directions on the close-packed planes of the solid and the substrate, respectively.²⁸ With *ab initio* MD simulations, Wang *et al.*²⁰ observed an fcc-like ordering in liquid Al at the interface with the Ti-terminated TiB₂ substrate, but not with B-terminated TiB₂. Our previous studies^{21,22} reveal that the atomic layering is independent of f , but the in-plane atomic ordering degrades with an increase in f . Furthermore, we found that the substrate lattice can induce the 2D ordered structure at the interface, similar to the “prefreezing” Pb layers^{19,29} and fcc-like ordering.²⁰ All the studies suggest that the liquid atoms at the interface is no longer disordered, where the atomic ordering is distinct from the bulk liquid and highly dependent on the structural and chemical properties of the substrates.

The substrate-induced prenucleation may promote heterogeneous nucleation in solidification if the 2D ordered structure at the interface has a good lattice matching with a new phase or retard nucleation if it has a wrong atomic structure. The potency of the substrate initially degrades with an increase in absolute value of f for $-12.5\% < f < 12.5\%$, attributed to the deterioration of the matching due to an increase in the density of misfit dislocations at the interface.^{22,28,31} For example, with *ab initio* MD simulations, Wang *et al.*²⁰ observed that the growth of α -Al was frustrated by the

f (−4.2%) between bulk Al and TiB₂ at an undercooling of about 2 K. With a monolayer of Al₃Ti formed on the basal plane of TiB₂, f reduces from −4.2 to 0.09% for α -Al/Al₃Ti. Consequently, the TiB₂ particle becomes very potent to nucleate α -Al with an undercooling of about 0.02 K.³² A further increase in f will introduce the coincidence site lattice (CSL) at the interface, which accommodates the major part of f and transforms the original substrate into a considerably potent nucleant.^{33,34} On the other hand, with *in situ* x-ray scattering, Schüllli *et al.*³⁵ found that Au atoms exhibited the pentagonal atomic arrangement in AuSi eutectic droplets at the interface with the (111) Si substrate, which was inconsistent with fcc-Au and caused a lateral-ordering stabilization process and then acted as the main barrier for heterogeneous nucleation. Therefore, prenucleation may dramatically change the potency of a substrate and have a profound effect on the subsequent heterogeneous nucleation.

Prenucleation could be eliminated partially or almost completely by impeding the “hard wall” effect and/or structural templating mechanism. The atomic layering at the interface can be suppressed by the surface roughness for both amorphous and crystalline substrates and be completely eliminated by the rough surface of the bulk amorphous substrate.^{26,27} The in-plane atomic ordering can be eliminated by an amorphous substrate, regardless of the surface roughness, for the disordered structure of the amorphous substrate may thoroughly impede the structural templating mechanism.²⁷ On the other hand, some in-plane atomic ordering persists at the interface with the crystalline substrate even with the atomic-level roughness of 100%, where the surface layer of the crystalline substrate still provides some equilibrium atomic positions for liquid atoms and the structural templating mechanism can work in a certain degree.²⁷ Therefore, the amorphous substrate could be the worst candidate for heterogeneous nucleation since it reduced the lattice matching between the substrate and new phase to the least. The study on the nucleation of the liquid on the amorphous substrates may tell us where the boundary between homogeneous and heterogeneous nucleation lies.

In this study, we intend to examine the nucleation of liquid Al adjacent to the amorphous substrates. Aluminum is a representative simple metal with free electrons and has extensive applications as a light metal in industries. The deepest undercooling of 175 K for pure liquid Al is achieved by the thermal analysis measurements on powder dispersions.³⁶ The atomistic simulations on homogeneous and heterogeneous nucleation of liquid Al have been carried out intensely.^{20,22,31,37–43} The objective of this study was to investigate the atomistic mechanism of nucleation in liquid Al in contact with the amorphous substrates with atomic-level smooth or rough surfaces and to establish the boundary between homogeneous and heterogeneous nucleation if it exists.

II. SIMULATION APPROACH

The embedded atom method (EAM) potential for aluminum, developed by Zope and Mishin to model interatomic interactions,⁴⁴ was used in this work. The predicted melting temperature for pure Al is 870 ± 4 K with this potential,⁴⁴ which is about 50 K lower than the experimental value (933 K). This difference is not unusual for the prediction of the melting point with empirical potentials. For a

study of generic properties of nucleation, the exact potential model does not matter since we only take the nucleation undercooling (the difference between the melting point and nucleation temperature) into consideration. The MD simulations were performed using the LAMMPS package.⁴⁵

The simulation systems of liquid Al/amorphous substrates with smooth or rough surfaces were constructed, with a total of 15 552 atoms (3456 and 12 096 atoms in the substrate and liquid, respectively). The liquid Al was prepared by heating the Al slab to 1500 K with a temperature step of 50 K, equilibrating for 0.1 ns at each temperature step. The liquid Al was cooled to 900 K with a temperature step of 50 K and then further quenched to 0.1 K, equilibrating for 1 ns at each temperature step. Two types of amorphous substrates with rough surfaces were obtained by taking the chunk with 3 atomic layers thick from the bulk liquid Al, which is equilibrated at 900 and 0.1 K, respectively, and then freezing their atomic positions (the substrates were denoted as R1- and R2-substrate, respectively). Two types of amorphous substrates with smooth surfaces were obtained by freezing the x and y coordinates of the atoms in the same chunks and resetting the z coordinates as the z -direction center of the corresponding atomic layer (the substrates were denoted as S1- and S2-substrate, respectively). The amorphous substrate has a roughness of $R = 0\%$ for the smooth surface and 100% for the rough surface, according to our definition of surface roughness of the amorphous substrate.²⁷ The liquid Al slab, equilibrated at 900 K, was then brought close to the amorphous substrate to equilibrate at 900 K for 1 ns, while the atoms of the substrate were fixed. Our previous unpublished study suggests that the fixed substrate only produces a negligible effect on both the interfacial structure of the liquid at equilibrium and the nucleation process during solidification at the liquid/substrate interface. Periodic boundary conditions are imposed in three dimensions of the simulation system, and the Nose–Hoover NPT ensemble is used for temperature and pressure control with a damping time of 0.1 ps. It should be pointed out that different choices of the ensembles (such as NVT, NPT, and NP_zAT) would not produce significant difference on the simulation results as long as the setting up of the simulation is reasonable.^{29,34} During the simulations, the liquid Al atoms are allowed to move freely under the effect of the interatomic potential, and the substrate atoms are excluded from equations of motion, but the forces they exert on adjacent atoms are included. The equations of motion are integrated by means of the Verlet algorithm with a time step of 1 fs.

To determine the nucleation temperature, T_n , for each specified nucleation system, the variable step search method is used. First, the liquid Al/amorphous substrates are cooled to a desired temperature with a temperature step of 50 K, running for 2 or 5 ns at each temperature step, and the nucleation temperature, T_1 , is determined by monitoring the variation in the total energy of the simulation system. Then, a finer search between T_1 and $T_1 + 50$ K with a temperature step of 5 K is performed to determine the nucleation temperature, T_2 . Finally, the nucleation temperature, T_n , is determined by a further finer search between T_2 and $T_2 + 5$ K with a temperature step of 1 K. This approach allows T_n to be determined within ± 1 K, which is the highest temperature at which nucleation occurs during the simulations.

The atomic layering in the liquid adjacent to amorphous substrates is quantified using the atomic density profile, $\rho(z)$, along z direction as¹⁷

$$\rho(z) = \frac{\langle N_z \rangle}{L_x L_y \Delta z}, \quad (1)$$

where N_z is the number of atoms in the bin between $z - \Delta z/2$ and $z + \Delta z/2$ at time t , Δz is the bin width, a tenth of the layer spacing, the angled brackets indicate a time-averaged quantity, and L_x and L_y are x and y dimensions of the systems.

The atomic arrangements in the liquid are characterized by two approaches: the time-averaged atomic positions⁴⁶ and local bond-order analysis.⁴⁷ The time-averaged atomic positions of the individual atomic layers are taken within a period of 10 ps from a trajectory of the simulation systems, where the solid atoms usually vibrate at equilibrium positions and the liquid atoms move around, and so, we can distinguish the solid atoms from the liquid atoms.⁴⁶ Local bond-order analysis is another widely used method to identify the solid and liquid atoms during the nucleation or crystal growth in the atomistic simulations.⁴⁸ The local bond-order parameter, $q_l(i)$, is calculated as⁴⁷

$$q_l(i) = \left(\frac{4\pi}{2l+1} \sum_{m=-l}^l |q_{lm}(i)|^2 \right)^{\frac{1}{2}}, \quad (2)$$

where $(2l+1)$ dimensional complex vector $q_{lm}(i)$ is a sum of spherical harmonics, $Y_{lm}(r_{ij})$, over all the nearest neighboring atoms j of the atom i . Two neighboring atoms, i and j , can be recognized to connect if the correlation function, $q_6(i) \cdot q_6(j)$, exceeds a certain value, 0.1, in this study.²¹ An atom is identified to be solid if the number of connections that the atom has with its neighbors exceeds a threshold of 6.

The solid clusters are distinguished from bulk liquid with a time step of 1 ps during the simulation at T_n , using local bond-order analysis.⁴⁷ Similar to the forward flux sampling (FFS) method,^{49,50} a solid atom is considered to belong to one cluster if the distance from any other atom of this cluster is less than a threshold, which is an average of the nearest and second nearest atomic spacing at the corresponding T_n . The largest solid cluster is then selected at every time step by comparing the number of atoms for every cluster of the simulation system.

III. RESULTS

A. Effect of amorphous substrates on atomic ordering

Some preliminary results of the effects of amorphous substrates with smooth and rough surfaces on the atomic ordering have been published elsewhere.⁵¹ Figure 1(a) displays the front view of a snapshot of the liquid Al/S1-substrate at $t = 1$ ns during the simulation at $T = 900$ K. A layered structure persists in the liquid within a few atomic layers at the interface with a smooth surface of the amorphous substrate. The density profile, $\rho(z)$, of the simulation system is plotted as a function of the distance, z , away from the interface shown in Fig. 1(b). The amorphous substrate exhibits sharp peaks in the $\rho(z)$ curve. It is in accordance with the atomic structure of

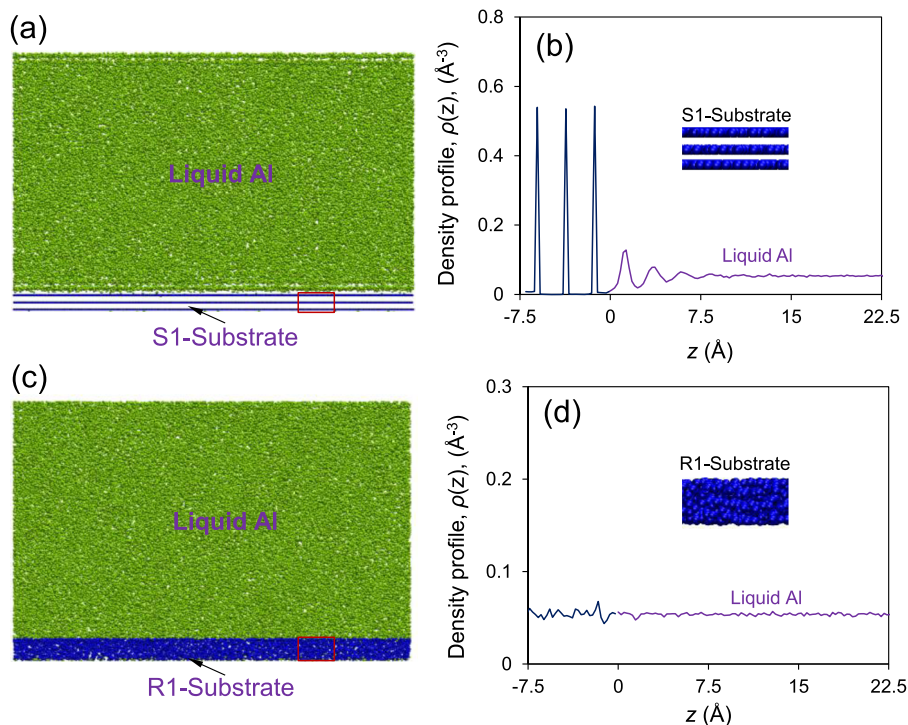


FIG. 1. Atomic layering. (a) The snapshot and (b) density profiles, $\rho(z)$, as a function of the distance, z , away from the interface for the liquid Al/S1-substrate, and (c) the snapshot and (d) $\rho(z)$ for the liquid Al/R1-substrate at $t = 1$ ns during the simulation at $T = 900$ K. The insets in (b) and (d) display the atomic arrangements of part of the amorphous substrates [enclosed by the boxes in (a) and (c)]. The liquid at the interface displays the atomic layering within about five atomic layers in the system with the S1-substrate and no layering with the R1-substrate.

the amorphous substrate with the smooth surface, where the atoms in the individual atomic layer are disordered in x and y directions and fixed at the center of the respective layer in the z direction, as shown in the inset of Fig. 1(b). The layering of the liquid at the interface extends about 5 atomic layers into the bulk liquid. The peak density of the first peak is 0.13 \AA^{-3} and then follows an exponential decrease away from the interface. A similar result can be observed for the liquid Al/S2-substrate (unshown here). This result is in a good agreement with our previous studies.^{26,27}

There is no layering in the liquid at the interface with the rough surfaces of amorphous substrates {R1-[Figs. 1(c) and 1(d)] or R2-substrate (unshown here)}. The R1-substrate has a disordered structure with the characteristics of bulk amorphous phase and a rough surface at an atomic level, as indicated by the constant $\rho(z)$ and shown in the inset of Fig. 1(d). The $\rho(z)$ curve extends smoothly from the amorphous substrate to bulk liquid, and no layered structure exists in the liquid at the interface.

We further investigate the formation of the atomic layering in the liquid contacted with the smooth surface of amorphous substrates (S1-substrate). At the beginning of the simulation ($t = 0$ ps) when the liquid is just brought close to the amorphous substrate with smooth surface [Fig. A1(a)], the liquid has a constant $\rho(z)$ of about 0.05 \AA^{-3} , which is similar to that of the bulk liquid and terminates sharply at the interface [Fig. A1(b)]. At $t = 1$ ps during the simulation at $T = 900$ K, the layered structure becomes visible within

3 atomic layers at the interface [Figs. A1(c) and A1(d)]. Further examination reveals that such a density profile gradually forms in a very short time (less than 1 ps) (Fig. A2). The first peak emerges on the $\rho(z)$ within the first 50 fs, followed by the second peak at 100 fs and the third peak at 500 fs. The peak density of the individual peak continuously increases with t during the simulation of the first 1 ps. The first peak reaches a peak density of 0.12 \AA^{-3} at $t = 1$ ps, which remains almost constant during the rest of the simulation. Therefore, the formation of atomic layering at the interface might be attributed to the self-organization of liquid atoms in contact with the smooth surface of amorphous substrates, which only requires a slight adjustment in the individual atomic position with a relaxation time of about 30 fs.^{52,53}

The radial distribution functions (RDFs) are then calculated to characterize the atomic structures of the liquid and amorphous substrates. The surface layer (A1) of the S1-substrate exhibits a sharp first peak and a diffuse second peak on the RDFs [Fig. 2(a)], typical for amorphous phases that only have the short-range order (SRO). The first (L1) and second (L2) atomic layers in the liquid in contact with the S1-substrate have similar patterns as the A1 on the RDF [Figs. 2(b) and 2(c)], indicating that the atomic structures of the liquid at the interface are disordered, although there exists the layering. It is almost identical to the RDFs of A1, L1, and L2 in the system with the R1-substrate,⁵¹ which has the characteristics of bulk amorphous phase. On the other hand, A1 of the S2-substrate shows a

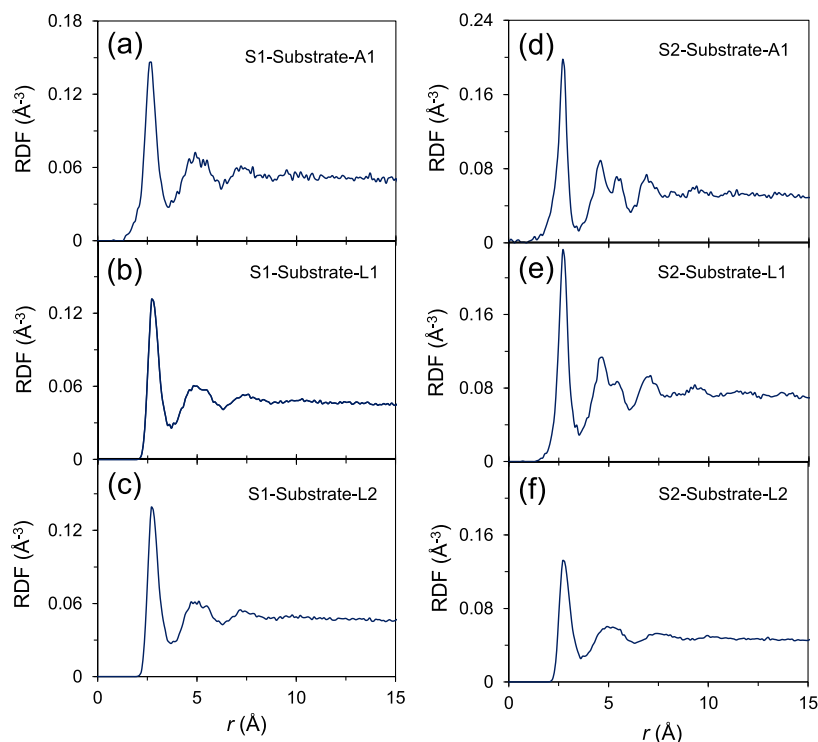


FIG. 2. Radial distribution functions, RDFs. The RDFs are plotted as a function of distance, r , for (a) the first layer (A1) of the substrate; (b) the first (L1) and (c) second (L2) atomic layers of the liquid in contact with S1-substrate; and (d) A1, (e) L1, and (f) L2 with the S2-substrate, equilibrated at $T = 900$ K. A shoulder or splitting of the second peak appears on the RDFs of A1 and L1 in the system with the S2-substrate.

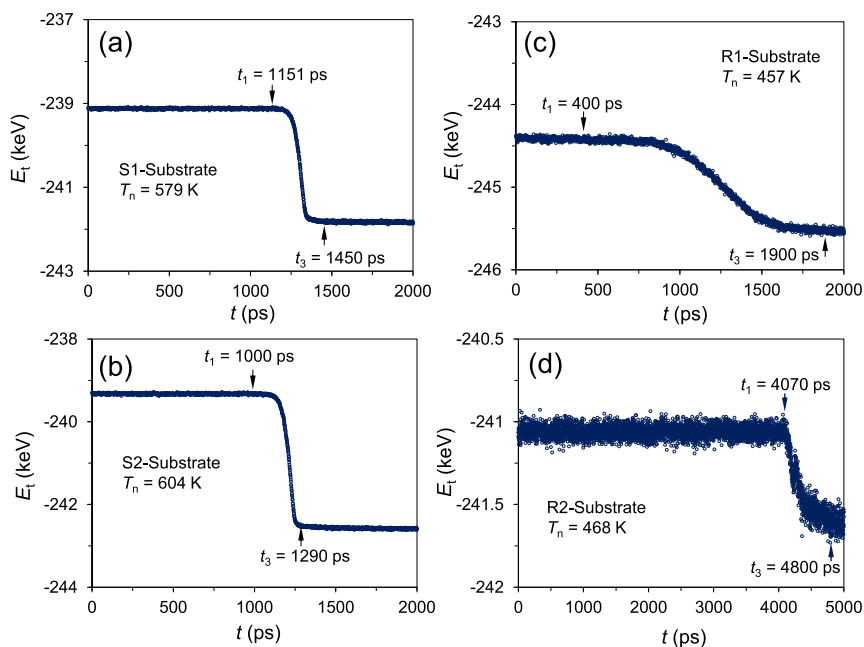


FIG. 3. Changes in the total energy, E_t , during the nucleation and growth. The value of E_t is plotted as a function of t during the simulations at (a) $T_n = 579$ K for the simulation system with the S1-substrate, (b) 604 K with the S2-substrate, (c) 457 K with the R1-substrate, and (d) 468 K with the R2-substrate. In addition, t_1 and t_3 mark the onset of nucleation and the end point of solidification, respectively.

splitting/shoulder of the second peak on the RDF, while the first peak remains sharp [Fig. 2(d)], indicative of the medium-range order (MRO) in the S2-substrate due to the lower quenching temperature. It is noted that the second peak on the RDF of the L1 displays a shoulder [Fig. 2(e)] and is diffused on that of the L2 [Fig. 2(f)], suggesting that the MRO in the S2-substrate further induces the in-plane MRO in L1. The MRO exists in the A1 of the R2-substrate as well [Fig. A3(a)], but cannot induce any MRO in the liquid at the interface with a rough surface of amorphous substrates [Figs. A3(b) and A3(c)].

We conclude that the smooth surface of amorphous substrates can induce the atomic layering and some local ordered structures (e.g., in-plane MRO) in the liquid at the interface and the rough surface eliminates any atomic ordering beyond the SRO. It should be pointed out that interfacial atomic ordering could be blurred by the mesoscopic fluctuation of liquid atoms at the interface due to the capillary waves, and the layering oscillations at the interface may be recovered by the intrinsic surface (interface) structure.⁵⁴ In this study, however, the rough surfaces of amorphous substrate have the inherent (atomic-level) disordered structure of bulk amorphous, which prevents the existence of any mesoscopic fluctuations of liquid atoms at the interface. We believe that the intrinsic surface (interface) structure of the liquid adjacent to the amorphous substrates with the rough surface should be identical to the density profile calculated in the present study. Thus, one expects that in the amorphous substrates with the rough surface, it is impossible to provide assistance for promoting the nucleation of any ordered phases in the liquid and so homogeneous nucleation will take place. The question is whether or not the atomic ordering and the local ordered structures in the liquid at the interface, induced by the smooth surface of amorphous substrates, can facilitate heterogeneous nucleation under large undercooling

B. Effect of amorphous substrates on heterogeneous nucleation

The nucleation temperature, T_n , has been determined to be 579 and 604 K for the liquid Al with S1-substrate [Fig. 3(a)] and S2-substrate [Fig. 3(b)], respectively, which is equivalent to the nucleation undercooling, ΔT_n , of 291 and 266 K, respectively. We take the simulation on the liquid Al/S1-substrate for further examination. At $T_n = 579$ K, the nucleation occurs at about $t_1 = 1151$ ps, where the total energy, E_t , starts to decrease. The solidification of the system is completed at about $t_3 = 1450$ ps and the E_t levels off after t_3 [Fig. 3(a)]. t_1 and t_3 are determined by the turning points of the first derivative of the E_t with respect to t , marking the onset of nucleation and the end of solidification, respectively.

The largest solid clusters in the simulation system were identified with a time step of 1 ps during the simulations at T_n , using local bond-order analysis. The number of atoms, N_{largest} , in the largest clusters was plotted as a function of t for the liquid Al/S1-substrate during the simulation at $T_n = 579$ K as shown in Fig. 4. The N_{largest} curve initially exhibits a baseline of about 20, with spikes on top of it, and then increases dramatically after $t = 1151$ ps [Fig. 4(a)]. The insets in Fig. 4(a) show the atomic arrangements of the largest clusters at some spikes with the local maximum N_{largest} , where N_{largest} is labeled. The largest solid cluster usually has an irregular

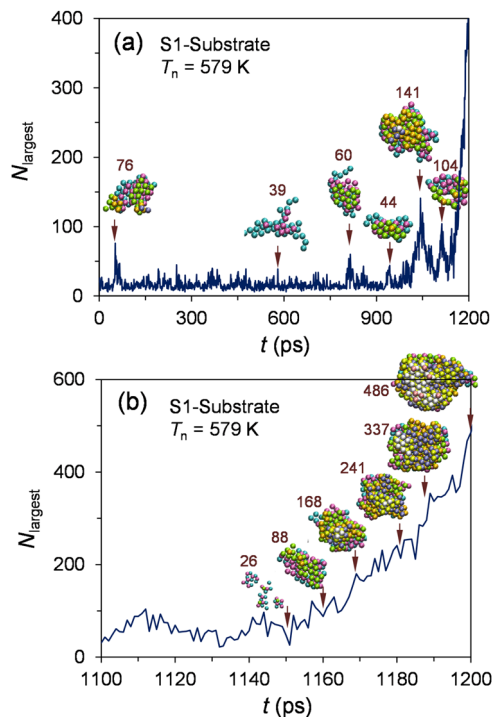


FIG. 4. Variations of the largest solid clusters/growing nucleus with t on the smooth surface of the amorphous substrate. The number of atoms, N_{largest} , in the largest clusters is plotted as a function of t from (a) $t = 0$ –1200 ps and (b) 1100–1200 ps for the liquid Al/S1-substrate during the simulation at $T_n = 579$ K. The inserts are the images of the largest cluster/growing nucleus with N_{largest} labeled. From $t = 1151$ ps, the largest cluster continuously grows into a regular spherical cap, indicating the formation of the nucleus.

morphology, and N_{largest} changes between tens to more than 100 with t . It suggests that these solid clusters are not stable, forming and collapsing instantly. After $t = 1151$ ps, the largest cluster steadily grows and develops into a regular spherical cap [Fig. 4(b)], indicative of the formation of the nucleus.

Most of the solid clusters, especially the largest, form at the interface with the smooth surface of amorphous substrate. Figure 5 shows the side views of the snapshots of solid clusters in the liquid Al/S1-substrate during the simulation at $T_n = 579$ K. The largest solid clusters in the snapshots of $t = 982$ ps [Fig. 5(e)], 1093 ps [Fig. 5(g)], 1132 ps [Fig. 5(j)], and 1151 ps [Fig. 5(k)], corresponding to the valleys of the N_{largest} curve shown in Fig. 4(a), are apparently smaller than those on the peaks (for all other t shown in Fig. 5). From 1150 ps, the largest cluster on the surface of the bottom amorphous substrate continues to grow into a regular spherical cap [Figs. 5(k)–5(p)]. It suggests that the amorphous substrate with the smooth surface activates heterogeneous nucleation in the liquid Al at the interface.

Figure 6 shows the top views of the solid clusters at the surface of the bottom S1-substrate, superimposed on the A1, during the simulation at $T_n = 579$ K. For clarity, the enlarged images with the largest clusters/growing nucleus are shown in Fig. A4. Before

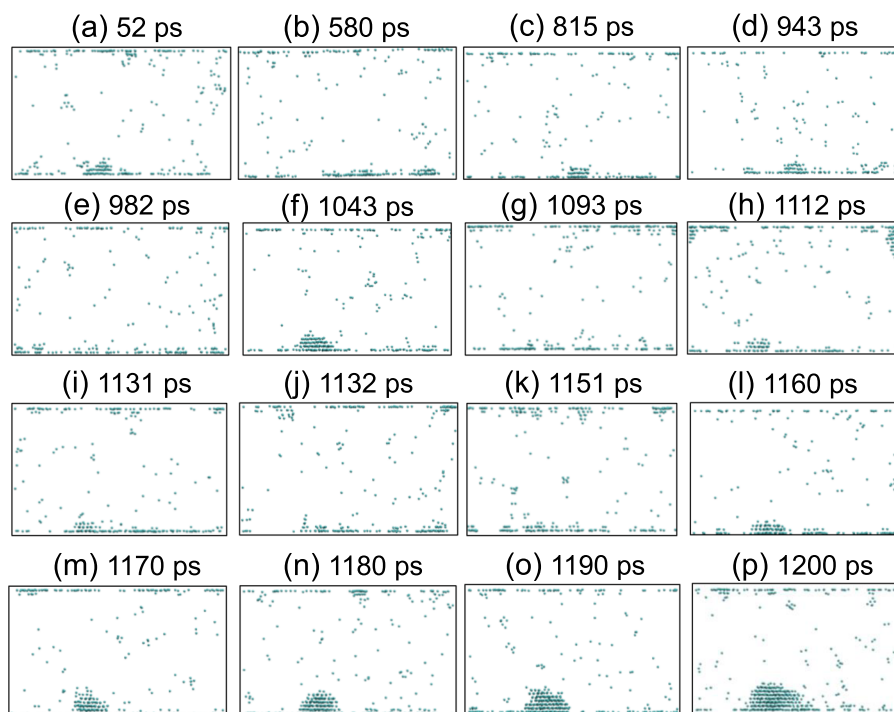


FIG. 5. The solid clusters/growing nucleus on the smooth surface of the amorphous substrate (side views). The side views of the snapshots of solid clusters in the liquid Al/S1-substrate at (a) $t = 52$ ps, (b) 580 ps, (c) 815 ps, (d) 943 ps, (e) 982 ps, (f) 1043 ps, (g) 1093 ps, (h) 1112 ps, (i) 1131 ps, (j) 1132 ps, (k) 1151 ps, (l) 1160 ps, (m) 1170 ps, (n) 1180 ps, (o) 1190 ps, and (p) 1200 ps during the simulation at $T_n = 579$ K. Most of the solid clusters, especially the largest, are formed at the interface, and from $t = 1151$ ps, the largest cluster on the surface of the bottom S1-substrate continues to grow into a regular spherical cap.

$t = 1151$ ps, the solid clusters with various sizes and morphologies are scattered randomly on the surface of the amorphous substrate [Figs. 6(a)–6(k)], and the size, morphology, and positions of the largest clusters change with t (Figs. A4(a)–A4(j)). These largest clusters at $t = 982$, 1093, 1132, and 1151 ps, corresponding to the valleys of the N_{largest} curve shown in Fig. 4(a), are apparently smaller than others, which are at the peaks. From $t = 1151$ –1160 ps, the largest cluster merges with other nearby solid clusters [Figs. 6(k), 6(l), A4(j), and A4(k)] with an unregular shape, which should be attributed to the anisotropy in the interfacial energies of the L/S interface.⁵⁵ The unregular nucleus continues to grow until the spherical cap forms at $t = 1200$ ps [Figs. 5(m)–5(p), 6(m)–6(p), and A4(l)–A4(o)]. It suggests that the nucleus has formed.

We further investigate how the amorphous substrate with the smooth surface triggers heterogeneous nucleation in the liquid Al at the interface. Figure 7 shows the time-averaged atomic positions of part of the L1/A1 in the liquid Al/S1-substrate within 10 ps from $t = 1140$ ps during the simulation at $T_n = 579$ K. Three solid clusters in L1 are highlighted by the envelopes with thick (purple online) lines. Inside the envelopes, the network of light (red online) lines, which connect the nearest neighboring atoms in A1, is indicative of the slightly distorted local fcc/hcp structure of the (111)/(0001) plane in L1/A1. The atoms in L1/A1 follow the ABC/AB stacking sequences of fcc/hcp structures. It suggests that the amorphous

substrate with the smooth surface can provide a certain degree of structural templating and induce the local ordered structure in the liquid Al at the interface. Statistically, it is reasonable that the amorphous substrate could exhibit varied local lattice structures with very small sizes. It becomes enhanced with decreasing the quenching temperature in the preparation of the amorphous substrates, as indicated by the MROs in the S2-substrate and R2-substrate. The local ordered structure induces the solid clusters/nucleus in the liquid at the interface with the best matching, e.g., the fcc-like clusters in liquid Al. The interface-induced atomic layering might be another factor to promote the formation of the solid clusters in the liquid, while the surface of amorphous substrates is smooth.

The atoms with fcc/hcp structures (solid atoms) were distinguished from those with disordered (liquid atoms) or other structures, according to the calculated local bond-order parameters of q_4 and q_6 . Figure 8(a) shows the top views of the atomic arrangements of solid atoms in L1 superimposed on A1 in the liquid Al/S1-substrate at $t = 1151$ and 1170 ps, respectively, during the simulation at $T_n = 579$ K. Most of the atoms in A1 have disordered structures (denoted as A1-dis) and some have an fcc (A1-fcc) or hcp (A1-hcp) structure. At $t = 1151$ ps, the solid atoms in L1 and the bulk liquid are located at either fcc or hcp atomic positions with equal probability [Fig. 8(a) and 8(b)]. After heterogeneous nucleation ($t = 1170$ ps), the solid atoms in the new phase dominantly occupy

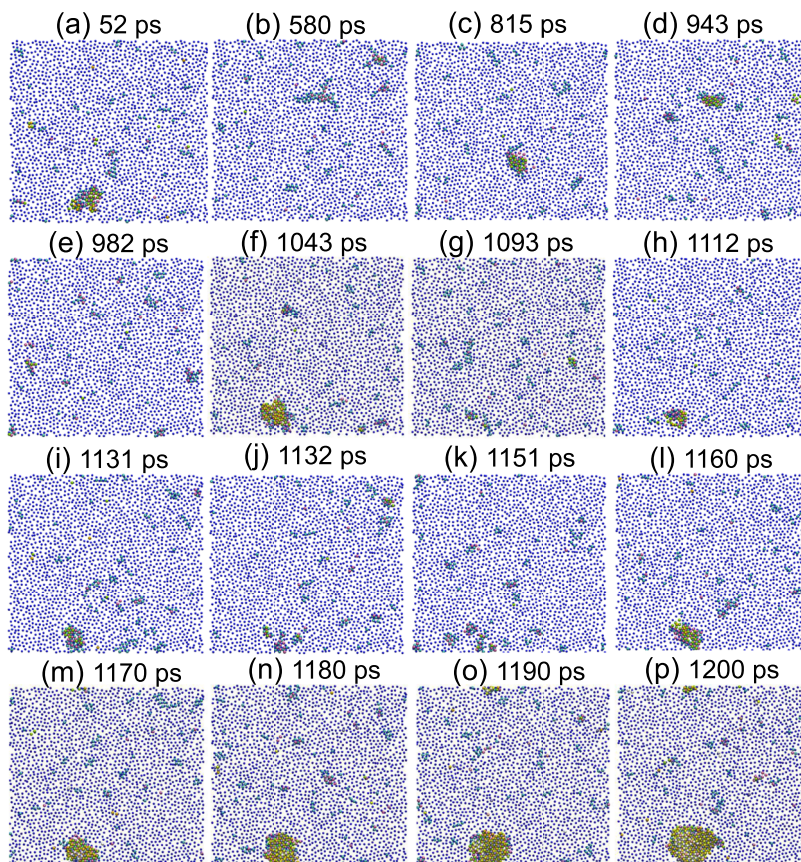


FIG. 6. Formation of the solid clusters/growing nucleus on the smooth surface of the amorphous substrate (top views). Top views of the snapshots of solid clusters on the surface layer (A1) of bottom substrate for the liquid Al/S1-substrate at (a) $t = 52$ ps, (b) 580 ps, (c) 815 ps, (d) 943 ps, (e) 982 ps, (f) 1043 ps, (g) 1093 ps, (h) 1112 ps, (i) 1131 ps, (j) 1132 ps, (k) 1151 ps, (l) 1160 ps, (m) 1170 ps, (n) 1180 ps, (o) 1190 ps, and (p) 1200 ps during the simulation at $T_n = 579$ K.

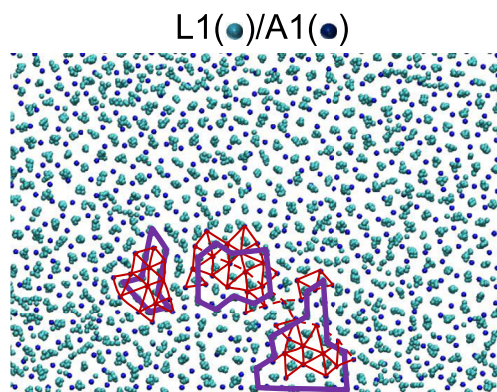


FIG. 7. Local ordered structure. The time-averaged atomic positions of part of L1/A1 within 10 ps from $t = 1140$ ps during the simulation at $T_n = 579$ K for the liquid Al/S1-substrate. The thick (purple online) lines envelop some local ordered structures in L1, and thin (red online) lines highlight the slightly distorted local fcc/hcp structures of the (111) plane in A1. The atoms with the local ordered structure in L1 are located at the lattice position provided by the underlying A1 atoms with slightly distorted local fcc/hcp structures.

the fcc lattice [Figs. 8(c) and 8(d)]. It suggests that nucleation and growth of fcc-Al is still favored even at an undercooling of as large as 291 K, where the slightly distorted (111)/(0001) lattice of local fcc/hcp structures in A1 has the best matching with the stable phase of α -Al.

C. Effect of amorphous substrates on homogeneous nucleation

The nucleation temperature is 457 and 468 K for the systems of liquid Al with R1-substrate and R2-substrate [Figs. 3(c) and 3(d)], respectively, equivalent to the ΔT_n of 413 and 402 K, respectively. It should be pointed out that a longer simulation time (5 ns) is necessary to observe the occurrence of the nucleation in the systems of liquid Al/amorphous substrates with rough surfaces. The nucleation occurs at about $t_1 = 400$ ps, and the solidification ends at about $t_3 = 1900$ ps in the liquid Al/R1-substrate system during the simulation at $T_n = 457$ K.

Figure 9 shows the side views of solid clusters in the liquid Al/R1-substrate during the simulation at $T_n = 457$ K. Before $t = 400$ ps, the solid clusters are randomly distributed in the entire

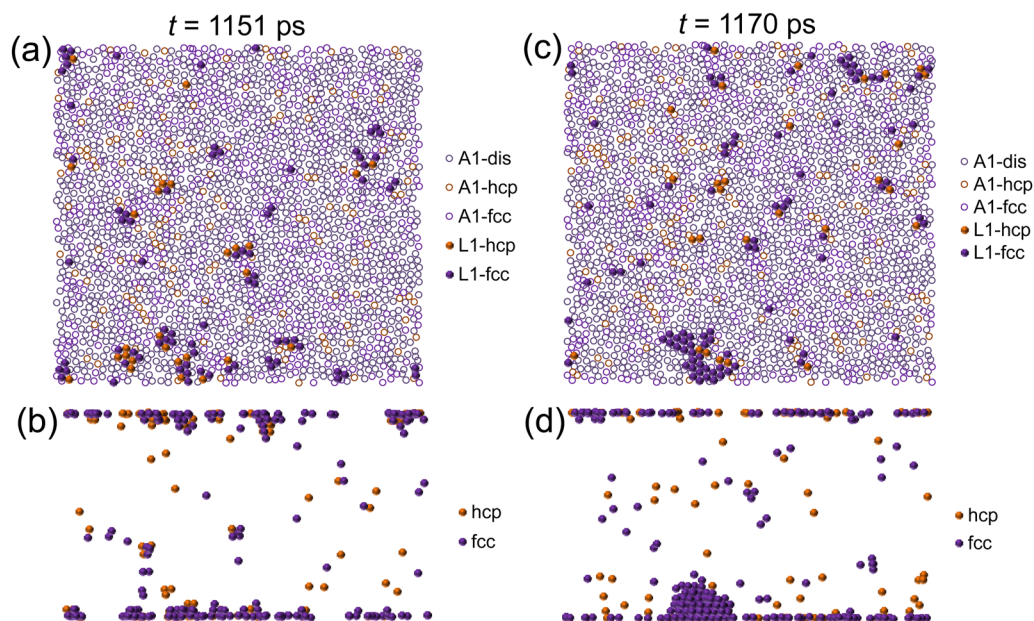


FIG. 8. Atomic arrangements of the solid atoms on the smooth surface of the amorphous substrate. Top views of the atomic arrangements of the solid atoms in L1 superimposed on A1 and side views of all the solid atoms in the liquid Al/S1-substrate at (a) and (b) $t = 1151$ ps and (c) and (d) 1170 ps, respectively, during the simulation at $T_n = 579$ K. The solid atoms are located at the fcc/hcp positions in the solid clusters with equal probability and dominantly occupy the fcc positions in the growing nucleus.

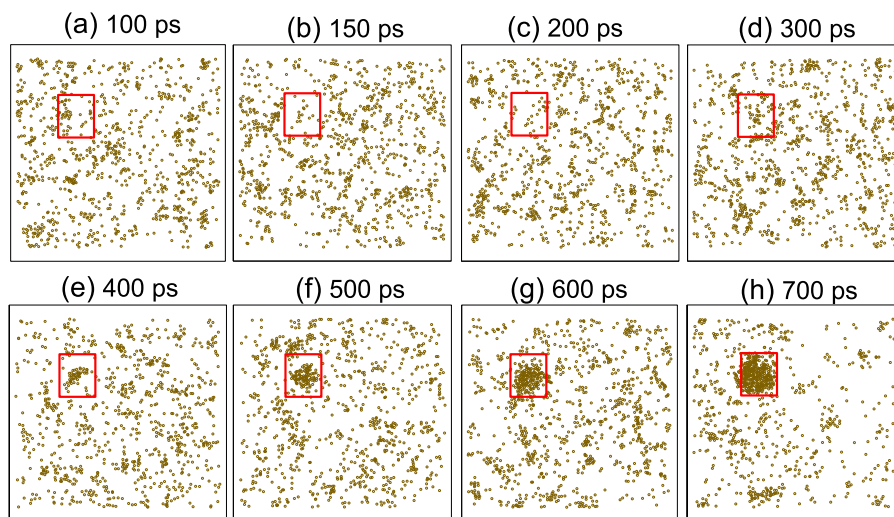


FIG. 9. Solid clusters in homogeneous nucleation. Side views of the solid clusters at (a) $t = 100$ ps, (b) 150 ps, (c) 200 ps, (d) 300 ps, (e) 400 ps, (f) 500 ps, (g) 600 ps, and (h) 700 ps for the liquid Al/R1-substrate during the simulation at $T_n = 457$ K. The (red online) box encloses the regions in which the nucleation occurs. One solid cluster in the highlighted region continues to grow from about $t = 400$ ps and develops into a sphere at about 700 ps, indicative of the occurrence of homogeneous nucleation.

space of the simulation system, with the sizes, morphologies, and positions changing with t [Figs. 9(a)–9(d)]. At $t = 400$ ps, one solid cluster with an irregular shape emerges in the region highlighted by a (red online) box [Fig. 9(e)] and then continues to grow into a sphere at about 700 ps [Figs. 9(f)–9(h)]. The location of this solid

cluster is far away from both the top and bottom amorphous substrates at this stage, indicating that its formation is irrelevant to the amorphous substrate. It indicates that the nucleus is created through the fluctuation mechanism in the bulk liquid, i.e., the nucleation is homogeneous.

The N_{largest} curve of the liquid Al/R1-substrate system has a flat baseline with an average N_{largest} of 14 before $t = 400$ ps during the simulation at $T_n = 457$ K (Fig. A5), where the largest N_{largest} of 33 appears at $t = 216$ ps. According to the CNT, the critical size of a nuclei ($2r^*$) for homogeneous nucleation in liquid Al is 1.3 nm at the undercooling of $\Delta T_n = 413$ K, which is calculated with the L/S interfacial energy of 0.158 J/m²⁵⁶ and entropy of fusion per unit volume of 1.112×10^6 J/Km³.⁵⁷ This nucleus includes about 69 atoms. The largest solid clusters before $t = 400$ ps in our simulation is much smaller than the nucleus. On the other hand, the average N_{largest} is about 22 in the liquid Al/S1-substrate system before $t = 1151$ ps during the simulations at $T_n = 579$ K, where the largest N_{largest} of 141 appears at $t = 1043$ ps [Fig. 4(a)]. It is noted that both the average and the largest N_{largest} before the nucleation in the liquid Al/S1-substrate system are significantly larger than that in the liquid Al/R1-substrate. The calculated $2r^*$ is 1.83 nm at $T_n = 579$ K, and the nucleus with a sphere shape includes about 189 atoms. In our simulation, the nucleus has a contact angle of about 90° with the smooth surface of the amorphous substrate, estimated from Fig. A6, and so, the number of the atoms in the nucleus reduces to 90. Therefore, the largest solid clusters induced by the smooth surface of the S1-substrate can reach the critical size of the nucleus and could start heterogeneous nucleation. The rough surface of amorphous substrates cannot provide any assistance to promote the nucleation in liquid Al.

D. Initial growth of nuclei

The initial growth rate of the nucleus was then examined for both heterogeneous and homogeneous nucleation. For heterogeneous nucleation, the N_{largest} of the liquid Al/S1-substrate system during the simulation at $T_n = 579$ K [Fig. 10(a)] was used to calculate the growth rate, N'_{largest} , in terms of the number of the atoms, as shown in Fig. 10(b). The N'_{largest} is zero before $t = 1151$ ps, as indicated by the dashed line. Then, it increases rapidly and reaches the peak at 1311 ps and afterward decreases dramatically. The radius, r , of the largest clusters/growing nucleus is obtained by converting the volume into a regular spherical cap and then used to calculate the growth velocity, V , as a function of t in terms of r , as shown in Fig. 10(c). Some subtle variations in the V curve can be observed. Before $t = 1151$ ps, the growth velocity oscillates around 0 Å/ps. It increases from 0 Å/ps at $t = 1151$ ps to 0.08 Å/ps (8 m/s) at $t = 1311$ ps and then decreases sharply. The transition of the V curve at $t = 1311$ ps is attributed to the impinging of the growing nucleus with its image in the simulation system due to the periodic boundary conditions (Fig. A6).

For homogeneous nucleation, the N_{largest} of the liquid Al/R1-substrate system during the simulations at $T_n = 579$ K [Fig. 11(a)] was used to calculate the growth rate, N'_{largest} , in terms of the number of the atoms. The N_{largest} remains very small with an average value of 14 before $t = 400$ ps, starts to increase slowly from $t = 400$ ps, and then accelerates after 600 ps. Correspondingly, N'_{largest} is zero before $t = 400$ ps. It increases gradually from 400 to 600 ps, speeds up until $t_2 = 898$ ps, and then begins to decline rapidly [Fig. 11(b)]. The growth velocity, V , in terms of r is plotted as a function of t as shown in Fig. 11(c). The V curve oscillates around 0 Å/ps before $t = 400$ ps, steadily increases from 0 Å/ps at $t = 400$ ps, and reaches a peak of 0.008 Å/ps (0.8 m/s) at 898 ps.

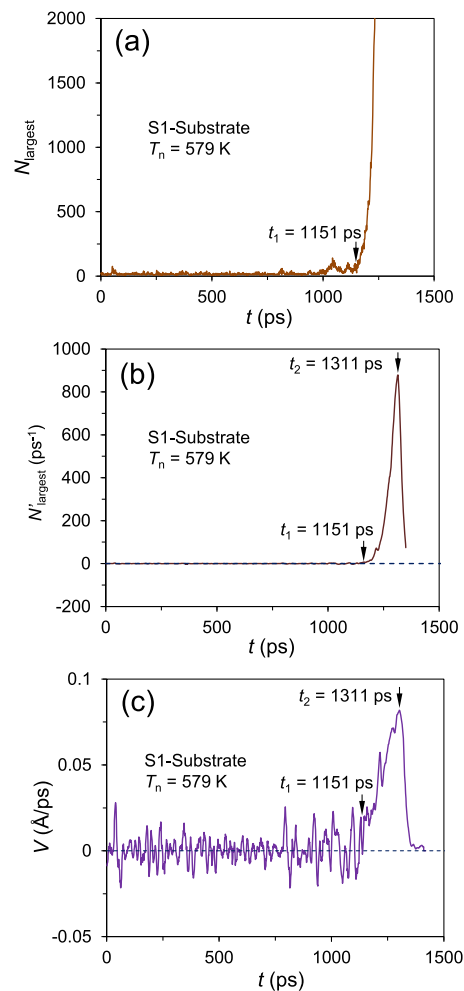


FIG. 10. Initial growth of the nucleus on the smooth surface of the amorphous substrate. (a) The number of atoms, N_{largest} , in the largest cluster/nucleus, (b) growth rates, N'_{largest} , in terms of the number of the atoms, and (c) growth velocity, V , in terms of the radius are plotted as a function of t for the liquid Al/S1-substrate during the simulation at $T_n = 579$ K. In addition, t_2 marks the point that the growing nucleus meets with its image in the simulation system. The growth rate V increases from 0 Å/ps at $t_1 = 1151$ ps, reaches the peak of 0.08 Å/ps at $t_2 = 1311$ ps, and then decreases sharply.

Some oscillations are visible on the V curve after $t = 400$ ps, where the change in the free energy of the nucleus is still positive in the initial stage of the growth. After $t = 898$ ps, the V decreases dramatically, due to the interaction of the growing nucleus with the surface of the top amorphous substrate.

For the first time, we reveal that the initial growth of the nucleus in heterogeneous nucleation at deep undercooling is much faster than that in homogeneous nucleation. The growth velocity, V , of the nucleus increases from 0 to 8 m/s in about 150 ps in heterogeneous nucleation at $\Delta T_n = 291$ K in the liquid Al adjacent to the smooth surface of the amorphous substrate. It is about 30 times faster than in the homogeneous nucleation occurring at $\Delta T_n = 413$ K. The V increases from 0 to 0.8 m/s in about 500 ps in the liquid Al with the

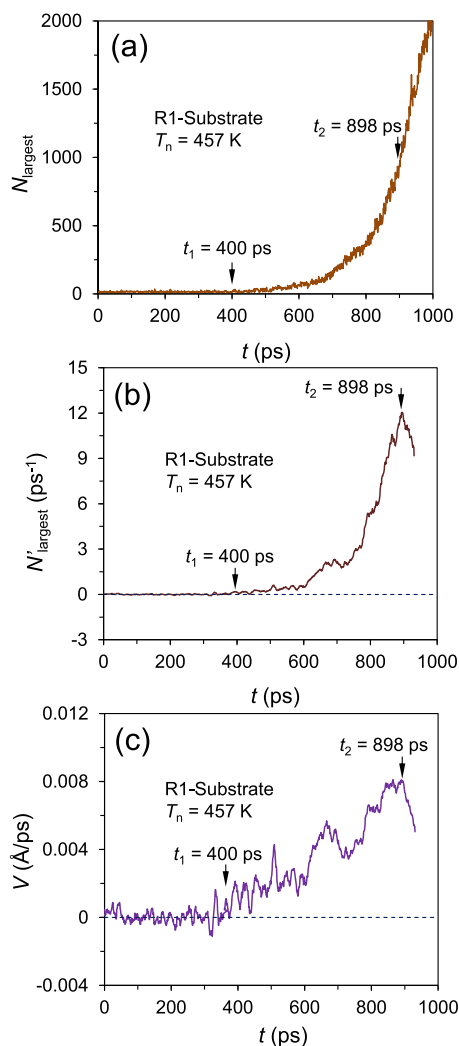


FIG. 11. Initial growth of the nucleus in homogeneous nucleation. (a) The number of atoms in the largest cluster/nucleus, N_{largest} , (b) growth rates, N'_{largest} , and (c) growth velocity, V , are plotted as a function of t for the liquid Al/R1-substrate during the simulations at $T_n = 457$ K. The growth rate, V , starts to increase from 0 Å/ps at $t = 400$ ps and reaches the peak of 0.008 Å/ps at 898 ps.

rough surface of the amorphous substrate. The behavior of crystal growth far from T_m in pure liquid metals significantly differs from that near T_m .⁵⁸ Near T_m , the crystal growth kinetics is predominantly controlled by the free energy difference between crystalline and liquid phases, and the growth velocity increases nearly linearly with increasing ΔT .^{59,60} As the ΔT increases, the growth velocity of fcc metals reaches a maximum at about $\sim 0.7 T_m$ and then decreases due to the slow kinetics at the L/S interface at high undercooling.^{61–66} However, the slow growth kinetics alone cannot account for a reduction in V of more than one order of magnitude with a decrease in ΔT_n of only 122 K from heterogeneous to homogeneous nucleation. The smooth surface of the amorphous substrate could also facilitate the initial growth of the nucleus by providing the structural

templating mechanism at the interface, except for the promotion of nucleation.

IV. GENERAL DISCUSSION

Classical MD simulations provide a powerful tool to capture the microstructural details of the nucleation process in liquids with reliable potentials, relatively long simulation times (\sim ns), and large simulation systems (\sim sub- μm),^{29,37,38,67–69} and meanwhile significant progress has also been made in experimental observations.^{70–72} Some novel techniques of the atomistic simulations, such as umbrella sampling,^{73,74} metadynamics,⁷⁵ and FFS^{76,77}, have been developed to investigate homogeneous nucleation near T_m . However, the nucleation rate of homogeneous nucleation is too low near T_m , and, in practice, it only can occur at a very large undercooling if possible. Under deep undercooling, the phase selection and the growth kinetics of L/S interface in the nucleation may significantly differ from those near T_m .^{78–80} On the other hand, some particles, often unknown, in the real liquids trigger the nucleation heterogeneously at an undercooling smaller than that of homogeneous nucleation. Heterogeneous nucleation on these particles with the least potency or having the largest undercooling, is our interest in this study. Thus, the classical MD simulation with a brute force approach might be the right choice for the study on the atomistic mechanism of either homogeneous or heterogeneous nucleation at a very large undercooling. Some techniques of the FFS are employed to investigate the nucleation process in this study. We have demonstrated that homogeneous nucleation occurred at an undercooling of larger than 400 K in the liquid Al/amorphous substrates with rough surface systems, more than 100 K larger than that of heterogeneous nucleation occurring at the interface with the smooth surface of amorphous substrates. Both are much larger than the deepest undercooling (175 K) for pure liquid Al that is achieved so far by experimental measurements.³⁶ This result justified our approaches used in this study.

This study reveals that a boundary exists between heterogeneous and homogeneous nucleation. Our study suggests that heterogeneous nucleation proceeds by the structural templating mechanism in the liquid at the interface with the substrates. The efficiency of the structural templating mechanism, namely, the potency of the substrate, largely depends on the degree of the matching between the substrate and new phase. It degrades with an increase in the lattice misfit of up to 12.5%.³¹ However, the potency of the substrate does not deteriorate further by increasing the misfit beyond 12.5%, and the coincidence site lattice at the interface will provide a good matching between the substrate and the new phase and transform the original substrates into a considerably potent nucleant.^{33,34} The worst scenario for heterogeneous nucleation is the liquid in contact with the amorphous substrate, which has the disordered structure. In this case, the local ordered structures in the amorphous substrates with the smooth surface still can induce the solid clusters at the interface by the structural templating mechanism, which may develop into the nucleus at high undercooling. On the other hand, the amorphous substrates with the rough surface prevent the formation of any atomic ordering in the liquid at the interface and contribute nothing to the nucleation. As a consequence, the fluctuation mechanism is responsible for the nucleation in the bulk liquid under the larger undercooling. This point is the boundary between

heterogeneous and homogeneous nucleation, i.e., the structural templating mechanism for the former and, in its absence, the fluctuation mechanism for the latter.

Our simulation results are supported by a recent study of the synthesis of the high-entropy alloy nanoparticles (HEA-NPs) assisted with liquid metal Ga,⁸¹ where the BCC-structure HEA-NPs form on the surface of Ga nanoparticles under mild conditions (the samples are naturally cooled down from $T = 923$ K to room temperature at a relatively low cooling rate). The liquid metal Ga endowing negative mixing enthalpy with other elements provides a stable thermodynamic condition for a desirable dynamic mixing reservoir with a uniform elemental distribution.⁸¹ The surface-induced atomic layering in the liquid metals, such as Hg, Ga, and Sn, has been observed.^{82–84} It is highly likely that the surface tension of liquid Ga nanoparticles induces the local ordered structure in the outmost atomic layer of the layered structure, which provides the structural templating mechanism and promotes heterogeneous nucleation of the HEA in the solidification at mild condition. Otherwise, in the case of homogeneous nucleation, the high cooling rate will be required to preserve the high-entropy state by quenching the melts. The attractive interactions between Ga and other elements will also facilitate heterogeneous nucleation⁸⁵ but not homogeneous nucleation. Without the structural templating mechanism, the chemical attractions will stabilize the liquid structure and frustrate the nucleation. Therefore, our study provided insights into the mechanism of the synthesis of the HEA-NPs assisted with liquid metal Ga.⁸¹

The structural templating seems to be a general atomistic mechanism of heterogeneous nucleation.^{22,29,31,33,34,86} Even above T_m , the substrates may induce the 2D ordered structure at the interface by the structural templating mechanism, i.e., prenucleation.^{21,23} On undercooling, heterogeneous nucleation proceeds by merging the pre-existing 2D ordered structures to form the nuclei at T_n .^{22,31,33,34} This process should be much easier than the fluctuation mechanism, for which the nucleus needs to be created from the disordered liquid at the interface, as described by the CNT. Thus, the actual kinetics of heterogeneous nucleation would be much faster than the prediction of the CNT. It is interesting to note that the nucleation rates extracted from the experiments are larger than those from either theoretical predictions or computer simulations in almost all cases.^{6,7,87–89} For example, Turnbull⁷ found that the predicted nucleation rate in mercury droplets could be five order of magnitudes lower than the experimental value for homogeneous nucleation, and 35 order of magnitudes lower than that for heterogeneous nucleation. The homogeneous nucleation rates in water from the experiments are 5–10 orders of magnitude higher than that from the computer simulations at medium undercooling.⁶ This has been attributed to the inherent uncertainty in the CNT (such as capillary approximation), the presence of impurity in the experiments or the inaccuracy of potentials used in the simulations, and so on.^{2,6,87} Our study indicates that the structural templating mechanism, instead of the fluctuation mechanism, should be responsible for heterogeneous nucleation, and this might largely account for the big deviation of experimental results from the prediction of CNT in the case of heterogeneous nucleation. In fact, the liquid atoms at the interface are no longer disordered,^{13,21,23} and the prerequisite of the fluctuation mechanism cannot be satisfied. Therefore, it is more

reasonable to describe heterogeneous nucleation with the structural templating mechanism, rather than the fluctuation mechanism. On the other hand, the present study reveals that some impurities in liquid, which is originally believed to be impotent, may be activated for heterogeneous nucleation and serve as an import factor for the disagreements between the experiment measurements and prediction of CNT/computer simulations in the case of homogeneous nucleation.

V. SUMMARY

In this study, we investigated the effects of amorphous substrates with smooth or rough surfaces on the atomistic mechanism of the nucleation and initial growth of the nuclei in liquid Al, with the MD simulations. It reveals that the slightly distorted local fcc/hcp structures in the amorphous substrates with smooth surfaces induce the local-ordered structures in the liquid at the interface through the structural templating mechanism. It further promotes the formation of the solid clusters on undercooling and subsequent heterogeneous nucleation at high undercooling of less than 300 K. On the other hand, the amorphous substrates with rough surfaces are irrelevant to the creation of the nucleus in liquid, and homogeneous nucleation occurs at an undercooling of more than 400 K through the fluctuation mechanism. The initial growth of the nuclei on the smooth surface of amorphous substrate can reach a growth velocity of 0.8 m/s within 150 ps, which is at least one order of magnitude faster than that in the system with the rough surfaces, which increases from 0 to 0.08 m/s within 600 ps. This study suggests that amorphous phase could be activated for heterogeneous nucleation, and the structural templating mechanism might be better to describe heterogeneous nucleation than the fluctuation mechanism. We establish that the structural templating is a general mechanism for heterogeneous nucleation, which sets the boundary between homogeneous and heterogeneous nucleation.

SUPPLEMENTARY MATERIAL

The supplementary material is available in the online version of this paper.

ACKNOWLEDGMENTS

This work was supported by the EPSRC of the UKRI under Grant Nos. EP/N007638/1 and EP/S35296/1. We are grateful to the UK Materials and Molecular Modeling Hub for computational resources, which is partially funded by the EPSRC (Grant Nos. EP/P020194/1 and EP/T022213/1), and maintained with support from Brunel University London.

AUTHOR DECLARATIONS

Conflict of Interest

The authors have no conflicts to disclose.

Author Contributions

All authors contributed equally to this work.

Hua Men: Conceptualization (equal); Data curation (equal); Formal analysis (equal); Investigation (equal); Methodology (equal); Project administration (equal); Resources (equal); Supervision (equal); Validation (equal); Visualization (equal); Writing – original draft (equal); Writing – review & editing (equal).

DATA AVAILABILITY

The data that support the findings of this study are available within the article.

REFERENCES

- 1 K. F. Kelton and A. L. Greer, *Nucleation in Condensed Matter: Applications in Materials and Biology* (Pergamon, Oxford, 2010).
- 2 X. Y. Liu, *J. Chem. Phys.* **112**, 9949 (2000).
- 3 D. Turnbull and B. Vonnegut, *Ind. Eng. Chem.* **44**, 1292 (1952).
- 4 R. Becker and W. Doring, *Ann. Phys.* **416**, 719 (1935).
- 5 D. Turnbull and J. C. Fisher, *J. Chem. Phys.* **17**, 71 (1949).
- 6 G. C. Sosso, J. Chen, S. J. Cox, M. Fitzner, P. Pedevilla, A. Zen, and A. Michaelides, *Chem. Rev.* **116**, 7078 (2016).
- 7 D. Turnbull, *J. Chem. Phys.* **20**, 411 (1952).
- 8 J. H. Perepezko, *Mater. Sci. Eng.* **65**, 125 (1984).
- 9 K. F. Kelton, *Solid State Phys.* **45**, 75 (1991).
- 10 D. M. Herlach, R. F. Cochrane, I. Egly, H.-J. Fecht, and A. L. Greer, *Int. Mater. Rev.* **38**(6), 273 (1993).
- 11 D. M. Herlach, T. Palberg, I. Klassen, S. Klein, and R. Kobold, *J. Chem. Phys.* **145**, 211703 (2016).
- 12 W. H. Hofmeister, M. B. Robinson, and R. J. Bayuzick, *Appl. Phys. Lett.* **49**, 1342 (1986).
- 13 W. D. Kaplan and Y. Kauffmann, *Annu. Rev. Mater. Res.* **36**, 1 (2006).
- 14 S. H. Oh, Y. Kauffmann, C. Scheu, W. D. Kaplan, and M. Rühle, *Science* **310**, 661 (2005).
- 15 W. J. Huisman, J. F. Peters, M. J. Zwanenburg, S. A. de Vries, T. E. Derry, D. Abernathy, and J. F. van der Veen, *Nature* **390**, 379 (1997).
- 16 H. Reichert, O. Klein, H. Dosch, M. Denk, V. Honkimäki, T. Lippmann, and G. Reiter, *Nature* **408**, 839 (2000).
- 17 A. Hashibon, J. Adler, M. W. Finnis, and W. D. Kaplan, *Interface Sci.* **9**, 175 (2001).
- 18 A. Hashibon, J. Adler, M. W. Finnis, and W. D. Kaplan, *Comput. Mater. Sci.* **24**, 443 (2002).
- 19 J. P. Palafox-Hernandez, B. B. Laird, and M. Asta, *Acta Mater.* **59**, 3137 (2011).
- 20 J. S. Wang, A. Horsfield, U. Schwingenschlögl, and P. D. Lee, *Phys. Rev. B* **82**, 184203 (2010).
- 21 H. Men and Z. Fan, *Metall. Mater. Trans. A* **49**, 2766 (2018).
- 22 Z. Fan and H. Men, *Mater. Res. Express* **7**, 126501 (2020).
- 23 H. Men, C. M. Fang, and Z. Fan, *Metals* **12**, 1704 (2022).
- 24 S. E. Donnelly, R. C. Birtcher, C. W. Allen, I. Morrison, K. Furuya, M. H. Song, K. Mitsuishi, and U. Dahmen, *Science* **296**, 507 (2002).
- 25 J. Fischer and M. Methfessel, *Phys. Rev. A* **22**, 2836 (1980).
- 26 P. Geysersmans, D. Gorse, and V. Pontikis, *J. Chem. Phys.* **113**, 6382 (2000).
- 27 B. Jiang, H. Men, and Z. Fan, *Comput. Mater. Sci.* **153**, 73 (2018).
- 28 Z. Fan, *Metall. Mater. Trans. A* **44**, 1409 (2013).
- 29 J. P. Palafox-Hernandez and B. B. Laird, *J. Chem. Phys.* **145**, 211914 (2016).
- 30 Y. Yang, D. L. Olmsted, M. Asta, and B. B. Laird, *Acta Mater.* **60**, 4960 (2012).
- 31 Z. Fan, H. Men, Y. Wang, and Z. P. Que, *Metals* **11**, 478 (2021).
- 32 Z. Fan, Y. Wang, Y. Zhang, T. Qin, X. R. Zhou, G. E. Thompson, T. Pennycook, and T. Hashimoto, *Acta Mater.* **84**, 292 (2015).
- 33 H. Men and Z. Fan, *J. Chem. Phys.* **158**, 034506 (2023).
- 34 H. Men and Z. Fan, *Metals* **12**, 1583 (2022).
- 35 T. U. Schüllli, R. Daudin, G. Renaud, A. Vaysset, O. Geaymond, and A. Pasturel, *Nature* **464**, 1174 (2010).
- 36 B. A. Mueller and J. H. Perepezko, *Metall. Trans. A* **18**, 1143 (1987).
- 37 Z. Y. Hou, K. J. Dong, Z. A. Tian, R. S. Liu, Z. Wang, and J. G. Wang, *Phys. Chem. Chem. Phys.* **18**, 17461 (2016).
- 38 J. S. Wang, A. Horsfield, P. D. Lee, and P. Brommer, *Phys. Rev. B* **82**, 144203 (2010).
- 39 H. L. Zhang, Y. F. Han, Y. B. Dai, J. Wang, and B. D. Sun, *J. Phys. D: Appl. Phys.* **45**, 455307 (2012).
- 40 D. Wearing, A. P. Horsfield, W. W. Xu, and P. D. Lee, *J. Alloys Compd.* **664**, 460 (2016).
- 41 M. Papanikolaou, K. Salonitis, M. Jolly, and M. Frank, *Metals* **9**, 1217 (2019).
- 42 A. Mahata, M. A. Zaeem, and M. Baskes, *Modell. Simul. Mater. Sci. Eng.* **26**, 025007 (2018).
- 43 T. Fujinaga and Y. Shibuta, *Comput. Mater. Sci.* **164**, 74 (2019).
- 44 R. R. Zope and Y. Mishin, *Phys. Rev. B* **68**, 024102 (2003).
- 45 S. Plimpton, *J. Comput. Phys.* **117**, 1 (1995).
- 46 K. A. Jackson, *Interface Sci.* **10**, 159 (2002).
- 47 P. J. Steinhardt, D. R. Nelson, and M. Ronchetti, *Phys. Rev. B* **28**, 784 (1983).
- 48 J. Baumgartner, A. Dey, P. H. H. Bomans, C. Le Coadou, P. Fratzl, N. A. J. M. Sommerdijk, and D. Faivre, *Nat. Mater.* **12**, 310 (2013).
- 49 R. J. Allen, D. Frenkel, and P. R. ten Wolde, *J. Chem. Phys.* **124**, 024102 (2006).
- 50 R. J. Allen, C. Valeriani, and P. Rein ten Wolde, *J. Phys.: Condens. Matter* **21**, 463102 (2009).
- 51 H. Men and Z. Fan, *Metals* **12**, 1529 (2022).
- 52 D. B. Macleod, *Proc. Phys. Soc.* **50**, 788 (1938).
- 53 C. Desgranges and J. Delhommelle, *Phys. Rev. B* **78**, 184202 (2008).
- 54 P. Tarazona, E. Chacon, and F. Bresme, *J. Phys.: Condens. Matter* **24**, 284123 (2012).
- 55 J. J. Hoyt, M. Asta, and A. Karma, *Mater. Sci. Eng. R* **41**, 121 (2003).
- 56 N. Eustathopoulos, L. Coudurier, J. C. Joud, and P. Desre, *J. Cryst. Growth* **33**, 105 (1976).
- 57 *Smithells Metals Reference Book*, edited by E. A. Brandes, 6th ed. (Butterworths, London, 1983), p. 8-1.
- 58 W. Kurz, D. J. Fisher, and R. Trivedi, *Int. Mater. Rev.* **64**, 311 (2019).
- 59 M. Asta, C. Beckermann, A. Karma, W. Kurz, R. Napolitano, M. Plapp, G. Purdy, M. Rappaz, and R. Trivedi, *Acta Mater.* **57**, 941 (2009).
- 60 J. J. Hoyt and M. Asta, *Phys. Rev. B* **65**, 214106 (2002).
- 61 H. W. Wilson, *London, Edinburgh Dublin Philos. Mag. J. Sci.* **50**, 238 (1900).
- 62 J. Frenkel, *Kinetic Theory of Liquids* (Oxford University Press, 1946).
- 63 Y. Ashkenazy and R. S. Averbach, *Europhys. Lett.* **79**, 26005 (2007).
- 64 Y. Ashkenazy and R. S. Averbach, *Acta Mater.* **58**, 524 (2010).
- 65 S. R. Coriell and D. Turnbull, *Acta Metall.* **30**, 2135 (1982).
- 66 G. Sun, J. Xu, and P. Harrowell, *Nat. Mater.* **17**, 881 (2018).
- 67 Y. F. Bi, B. X. Cao, and T. S. Li, *Nat. Commun.* **8**, 15372 (2017).
- 68 Y. Shibuta, S. Sakane, E. Miyoshi, S. Okita, T. Takaki, and M. Ohno, *Nat. Commun.* **8**, 10 (2017).
- 69 Y. Shibuta, S. Sakane, T. Takaki, and M. Ohno, *Acta Mater.* **105**, 328 (2016).
- 70 K. F. Kelton, *Int. J. Microgravity Sci. Appl.* **30**, 11 (2013).
- 71 D. Gebauer, A. Völkel, and H. Cölfen, *Science* **322**, 1819 (2008).
- 72 J. H. Zhou, Y. S. Yang, Y. Yang, D. S. Kim, A. Yuan, X. Z. Tian, C. Ophus, F. Sun, A. K. Schmid, M. Nathanson, H. Heinz, Q. An, H. Zeng, P. Ercius, and J. W. Miao, *Nature* **570**, 500 (2019).
- 73 G. M. Torrie and J. P. Valleau, *Chem. Phys. Lett.* **28**, 578 (1974).
- 74 G. M. Torrie and J. P. Valleau, *J. Comput. Phys.* **23**, 187 (1977).
- 75 A. Laio and M. Parrinello, *Proc. Natl. Acad. Sci. U. S. A.* **99**, 12562 (2002).
- 76 R. Cabriolu and T. S. Li, *Phys. Rev. E* **91**, 052402 (2015).
- 77 G. C. Sosso, T. S. Li, D. Donadio, G. A. Tribello, and A. Michaelides, *J. Phys. Chem. Lett.* **7**, 2350 (2016).
- 78 P. R. ten Wolde, M. J. Ruiz-Montero, and D. Frenkel, *J. Chem. Phys.* **104**, 9932 (1996).

- ⁷⁹J. X. Yang, H. Gould, W. Klein, and R. D. Mountain, *J. Chem. Phys.* **93**, 711 (1990).
- ⁸⁰P. Rein ten Wolde and D. Frenkel, *Phys. Chem. Chem. Phys.* **1**, 2191 (1999).
- ⁸¹G. Cao, J. Liang, Z. Guo *et al.*, *Nature* **619**, 73–77 (2023).
- ⁸²O. M. Magnussen, B. M. Ocko, M. J. Regan, K. Penanen, P. S. Pershan, and M. Deutsch, *Phys. Rev. Lett.* **74**, 4444–4447 (1995).
- ⁸³M. J. Regan, E. H. Kawamoto, S. Lee, P. S. Pershan, N. Maskil, M. Deutsch, O. M. Magnussen, B. M. Ocko, and L. E. Berman, *Phys. Rev. Lett.* **75**, 2498–2501 (1995).
- ⁸⁴O. G. Shpyrko, A. Y. Grigoriev, C. Steimer, P. S. Pershan, B. Lin, M. Meron, T. Graber, J. Gerbhardt, B. Ocko, and M. Deutsch, *Phys. Rev. B* **70**, 224206 (2004).
- ⁸⁵C. M. Fang, H. Men, and Z. Fan, *Metall. Mater. Trans. A* **49**, 6231–6242 (2018).
- ⁸⁶Z. Fan and H. Men, *Metals* **12**, 1547 (2022).
- ⁸⁷J. Russo and H. Tanaka, *J. Chem. Phys.* **145**, 211801 (2016).
- ⁸⁸S. Auer and D. Frenkel, *Nature* **409**, 1020 (2001).
- ⁸⁹L. Fillion, R. Ni, D. Frenkel, and M. Dijkstra, *J. Chem. Phys.* **134**, 134901 (2011).